1 **Global assessment of climatic responses to the ozone-vegetation**

2 **interactions**

3

4 Xinyi Zhou[1], Xu Yue[1], Chenguang Tian[1], Xiaofei Lu[1]

5

6 [1] Jiangsu Key Laboratory of Atmospheric Environment Monitoring and Pollution

7 Control, Collaborative Innovation Center of Atmospheric Environment and Equipment

8 Technology, School of Environmental Science and Engineering, Nanjing University of

9 Information Science & Technology, Nanjing, 210044, China

10

11 *Corresponding author*: Xu Yue (Email: yuexu@nuist.edu.cn)

Abstract. The coupling between surface ozone (O_3) and vegetation significantly influences regional to global climate. O_3 uptake by plant stomata inhibits photosynthetic rate and stomatal conductance, impacting evapotranspiration through land surface ecosystems. Using the climate-vegetation-chemistry coupled ModelE2-YIBs model, we assess the global climatic responses to O_3-vegetation interactions during boreal summer of 2010s (2005-2014). High O_3 pollution reduces stomatal conductance, resulting in the warmer and drier conditions worldwide. The most significant responses are found in the eastern U.S. and eastern China, where local latent heat flux decreases by -8.17% and -9.48%, respectively. Consequently, surface air temperature rises by +0.33 °C and +0.56 °C, and sensible heat flux rises by +16.54% and +25.46% in the two hotspot regions. The O_3-vegetation interaction also affects atmospheric pollutants. Surface O_3 concentrations increase by +1.26 ppbv in eastern China and +0.98 ppbv in eastern U.S. due to the O_3-induced inhibition of stomatal uptake. With reduced atmospheric stability following the warmer climate, increased cloudiness but decreased relative humidity jointly reduce aerosol optical depth (AOD) over eastern China. This study suggests that vegetation feedback should be considered for a more accurate assessment of climatic perturbations caused by tropospheric O_3.

1 Introduction

Tropospheric ozone (O_3), one of the most detrimental air pollutants (Myhre et al., 2013), not only poses threats to human health (Norval et al., 2011; Nuvolone et al., 2018) but also induces phytotoxic effects to vegetation (Mills et al., 2007; Pleijel et al., 2007). When exposed to certain levels of O_3, plant photosynthesis and stomatal conductance is inhibited due to the O_3 oxidation of cellular, enzyme, and chlorophyll (Dizengremel, 2001; Fiscus et al., 2005; Jolivet et al., 2016). Consequently, the carbon assimilation of terrestrial ecosystems is limited (Yue and Unger, 2014; Oliver et al., 2018) and the land-air exchange rates of water and heat fluxes are altered (Lombardozzi et al., 2015).

Experimental studies have shown that the excessive O_3 exposure reduced both plant photosynthesis and stomatal conductance (Ainsworth et al., 2012; Lombardozzi et al., 2013). The reduction rates are dependent on the O_3 stomatal fluxes as well as the damaging sensitivities that vary among different vegetation types (Nussbaum and Fuhrer, 2000; Karlsson et al., 2004; Pleijel et al., 2004). Traditional exposure-based indexes like accumulated hourly O_3 concentrations over a threshold of 40 ppb (AOT40) are widely used to assess O_3-induced vegetation damage (Fuhrer et al., 1997). However, such statistical schemes fail to account for the dynamic adjustment of vegetation physiological processes. Taking into account the variability of plant sensitivities, different O_3 damage schemes were proposed to quantify the O_3 impacts on land carbon assimilation from regional to global scales (Anav et al., 2011; Lam et al., 2023; Lei et al., 2020). For example, Sitch et al. (2007) calculated the simultaneous damages to both photosynthesis and stomatal conductance based on the instantaneous O_3 stomatal uptake. In contrast, Lombardozzi et al. (2012) estimated the inconsistent reductions in plant photosynthesis and stomatal conductance using different response relationships to the cumulative O_3 stomatal uptake. Applications of different schemes resulted in a wide range of reductions in gross primary productivity (GPP) by 2-12% globally with regional hotspots up to 20-30% (Lombardozzi et al., 2015; Unger et al., 2020; Zhou et al., 2024).

The O_3-induced inhibition in stomatal conductance decreases dry deposition and consequently enhances surface O_3 concentrations (Clifton et al., 2020; Wesely and

59   Hicks, 2000; Zhang et al., 2006). Using the Sitch et al. (2007) scheme with high O_3

60   damaging sensitivities in the climate model ModelE2-YIBs, Gong et al. (2020) revealed

61   that O_3-vegetation interactions increased regional O_3 concentrations by 1.8 ppbv in the

62   eastern U.S., 1.3 ppbv in Europe, and 2.1ppbv in eastern China. As a comparison, Sadiq

63   et al. (2017) found a consistent but stronger positive feedback on O_3 concentrations in

64   these polluted regions using the scheme of Lombardozzi et al (2012) embedded in a

65   different climate model. Inclusion of O_3-vegetation interactions will cause stronger

66   damages to land carbon assimilation due to the feedbacks of both ecosystem and surface

67   O_3. On one hand, the damages to leaf photosynthesis inhibit plant growth and decrease

68   leaf area index (LAI), leading to higher reduction percentage in GPP compared to

69   simulations without LAI changes (Yue et al., 2020). On the other hand, the O_3

70   enhancement due to vegetation feedback may cause additional vegetation damage and

71   result in further GPP losses (Lei et al., 2021). As a result, the O_3-vegetation interactions

72   should be considered in the global estimate of O_3 damages to ecosystem functions.

73   In addition to affecting surface O_3, the O_3-vegetation interaction can also alter the

74   water and energy exchange between land and atmosphere. For example, Lombardozzi

75   et al. (2015) used the Community Land Model (CLM) and estimated that the cumulative

76   uptake of O_3 by the leaves resulted in reduction of 2.2% in transpiration but increase of

77   5.4% in runoff globally. Arnold et al. (2018) used the Community Earth System Model

78   (CESM) and found that plant exposure to O_3 could decrease the land-air moisture fluxes

79   and atmospheric humidity, which further reduced shortwave cloud forcing in polluted

80   regions and induced widespread surface warming up to +1.5 K. Two recent studies

81   utilized the WRF-chem model and revealed considerable warming and the associated

82   meteorological perturbations due to the O_3-vegetation interactions in China (Zhu et al.,

83   2022; Jin et al., 2023). However, all these modeling studies applied the same O_3

84   vegetation damage scheme proposed by Lombardozzi et al. (2012). It's necessary to

85   assess the climatic responses to O_3-vegetation interactions using different schemes so

86   as to explore the robust responses and the associated uncertainties.

87   In this study, we quantified the global impacts of O_3-vegetation interaction on

88   climatic conditions and surface air pollutants during 2010s using the Earth system

89   model NASA GISS ModelE2 coupled with Yale Interactive terrestrial Biosphere (YIBs)

90   model (Yue and Unger, 2015). This fully coupled framework was implemented with the

91   semi-mechanistic O_3 damage scheme proposed by Sitch et al. (2007), which calculated

92   aggregate O_3 damage to photosynthesis based on varied sensitivities to instant stomatal

93   O_3 uptake for eight plant functional types (PFTs). We performed sensitivity experiments

94   to quantify the responses of surface air temperature and precipitation to O_3-vegetation

95   interaction. The feedbacks to aerosols and O_3 concentrations were also examined.

96

2 Method

2.1 Model descriptions

99   The ModelE2-YIBs is a fully coupled climate-carbon-chemistry model combining

100   the NASA GISS ModelE2 with the YIBs vegetation model. ModelE2 is a general

101   circulation model with the horizontal resolution of 2°×2.5° in latitude and longitude

102   and 40 vertical layers up to 0.1 hPa. It dynamically simulates gas-phase chemistry (NO_x

103   - HO_x - O_x - CO - CH4 - NMVOCs), aerosols (sulfate, nitrate, black and organic carbon,

104   dust, and sea salt), and their interactions (Menon and Rotstayn, 2006). The radiation

105   module includes direct and indirect aerosol radiative effects and accounts for absorption

106   of multiple greenhouse gases (GHGs). For cloud optical parameters, it uses Mie

107   scattering, ray tracing, and matrix theory (Schmidt et al., 2006). The model outperforms

108   20 other IPCC-class climate models in simulating surface solar radiation (Wild et al.,

109   2013) and has been extensively validated for meteorological and hydrological variables

110   against observations and reanalysis data (Schmidt et al., 2014).

111   The YIBs model employs the well-established Farquhar model for leaf

112   photosynthesis and Ball-Berry model for stomatal conductance (Farquhar et al., 1980;

113   Ball et al., 1987) as follows:

$$A_{tot} = \min (J_c, \quad J_e, \quad J_s) \quad\quad (1)$$

$$g_s = m \frac{(A_{tot} - R_d) \times RH}{c_s} + b \quad\quad (2)$$

114   Here, the total leaf photosynthesis, denoted as A_{tot}, is calculated as the minimum value

115   among the ribulose-1,5-bisphosphate carboxylase-limited rate of carboxylation (J_c),

116   light-limited rate (J_e), and export-limited rate (J_s). The stomatal conductance (g_s) is

117   linked to the variations of A_{tot} with parameters such as dark respiration rate (R_d),

118   relative humidity (RH), and CO_2 concentration at the leaf surface (c_s). The model

119   simulates the biophysical processes of eight PFTs including tundra, C_3/C_4 grass,

120   shrubland, deciduous broadleaf forest, evergreen broadleaf forest, evergreen needleleaf

121   forest, and cropland. Different values are assigned to parameters *m* and *b* for each PFT

122   (Table S1). The carbon uptake by the leaf is then accumulated and allocated to different

123   organs to support the plant development with dynamical changes in LAI and tree

124   growth.

125

126   **2.2 The O_3-vegetation damage scheme**

127   The YIBs model employs a semi-mechanistic parameterization proposed by Sitch

128   et al. (2007) to estimate the impact of O_3 on photosynthesis through stomatal uptake.

129   The scheme applies an undamaged factor (F) to both A_{tot} and g_s as follows:

$$A_{totd} = A_{tot} \cdot F \tag{3}$$

$$g_{sd} = g_s \cdot F \tag{4}$$

130   where A_{totd} and g_{sd} are the unaffected photosynthesis and stomatal conductance

131   separately. The factor *F* is defined as:

$$F = 1 - a_h \cdot \max\left[F_{O3} - F_{O3,crit}, 0.0\right] \tag{5}$$

132   a_h is the high O_3 sensitivity coefficient and $F_{O3,crit}$ is the specific threshold for O_3

133   damages, both of which varies with vegetation types (Table S1).

$$F_{O3} = \frac{[O_3]}{R_a + \left[\frac{k_{O3}}{g_{sd}}\right]}, \tag{6}$$

134   where $[O_3]$ represents surface O_3 concentrations, R_a stands for the aerodynamic and

135   boundary layer resistance. The constant k_{O3}=1.67 is the ratio of stomatal resistance for

136   O_3 to that for water.

137

138   **2.3 Experiments**

139   To explore the coupled O_3-vegetation effect, we performed two sets of simulations

140   using the ModelE2-YIBs model. The control experiment "10NO3" was conducted

141   without the O_3 damages to vegetation. As a comparison, the sensitivity experiment

142   "10HO3" contained online O_3-vegetation interaction with high O_3 sensitivity. For both

143   experiments, the 2010s anthropogenic emissions for 8 species (BC, OC, CO, NH_3, NO_x,

144   SO_2, Alkenes, and Paraffin) from 8 economic sources (agriculture, energy, industry,

145   transportation, resident, solvent, waste, and international shipping) and biomass

146   burning source were collected from the Coupled Model Intercomparison Project phase

147   6 (CMIP6) (van Marle et al., 2017; Hoesly et al., 2018). The ensemble mean of monthly

148   sea surface temperature (SST) and sea ice fraction (SIC) simulated by 21 CMIP6

149   models during the time period 2005-2014 was employed as the boundary conditions.

150   The cover fraction of 8 PFTs (Fig. S1) were adopted from the land use harmonization

151   (LUH2) dataset (Hurtt et al., 2020). For each simulation, the model was run for 30 years

152   with the first 10 years used as the spin up. We calculated the average of the last 20 years

153   and focused on the boreal summer season (June-July-August, JJA) when surface O_3

154   reaches the maximum in one year. We explored the climatic responses to O_3-vegetation

155   interactions as the differences between "10HO3" and "10NO3" on the global scale with

156   the special focus over the hotspot regions such as eastern U.S. (30–40º N, 80–90 º W)

157   and eastern China (22.5–38º N, 106–122º E).

158

159   **2.4 Data for evaluations**

160   We evaluated the simulated air pollutants, carbon fluxes, and meteorological

161   variables using observational and reanalysis datasets. The worldwide observations of

162   O_3 concentrations were collected from three regional networks: Air Quality Monitoring

163   Network operated by Ministry of Ecology and Environment (AQMN-MEE) in China,

164   the Clean Air Status and Trends Network (CASTNET) in the U.S., and the European

165   Monitoring and Evaluation Programme (EMEP) in Europe. For the latter two networks,

166   we chose the average over 2009-2011, while for AQMN-MEE, the mean value of 2014-

167   2018 was used due to its establishment in 2013. The simulated aerosol optical depth

168   (AOD) was validated using satellite-based data from the Moderate Resolution Imaging

169   Spectroradiometer (MODIS) retrievals (Remer et al., 2005) for the years 2009-2011.

170   The simulated GPP was evaluated against the data product upscaled from the

171   FLUXNET eddy covariance measurements for 2009-2011 (Jung et al., 2009). The daily

172   temperature at 2m (T_{2m}) in 2009-2011 was obtained from the National Centers for

173   Environmental Prediction/National Center for Atmospheric Research (NCEP/NCAR)

174   reanalysis 1 (NCEP1) (Kalnay et al., 1996). For precipitation, we used the monthly data

175   from Global Precipitation Climatology Project (GPCP) (Huffman et al., 1997; Adler et

176   al., 2018). All these datasets were interpolated to the same resolution as ModelE2-YIBs

177   model. Normalized mean biases (NMBs) were applied to quantify the deviations of

178   simulations from observations as follows:

$$NMB = \sum_{i}^{n}(S_i - O_i)/\sum_{i}^{n}O_i \times 100\% \qquad (7)$$

179   Here, S_i and O_i represent the simulated and observed values, respectively. *n* denotes the

180   total grid number used in the comparisons.

181

182   **3. Results**

183   **3.1 Model evaluations**

184   We first evaluated the air pollutants simulated by the ModelE2-YIBs model (Fig.

185   1). Over a total of 491 grids with site-level O_3 measurements (Fig. 1b), the model

186   adequately replicated both the magnitude and spatial distribution of the maximum daily

187   8-hour average (MDA8) O_3 concentrations ([O_3]), with correlation coefficient (r) of

188   0.58 and NMB of -1.27% (Fig. 1c). Simulated summertime surface [O_3] was high in

189   regions with large anthropogenic emissions, such as western Europe and eastern China

190   (Ohara et al., 2007), as well as in central Africa with frequent fire emissions (van der

191   Werf et al., 2017). On the global scale, the model yielded an average [O_3] of 44.36 ppbv

192   and observations showed an average of 44.57 ppbv over the same grids. However, the

193   modeled result is overestimated over the North China Plain and slightly underestimated

194   over the U.S. Simulated AOD at 550 nm (Fig. 1d) showed similar spatial pattern as the

195   satellite retrievals (Fig. 1e) with a high R=0.77 and low NMB of -6.27% globally (Fig.

196   1f). Both the simulations and observations showed AOD hotspots over North Africa

197   and the Middle East where dust emissions dominate, and in northern India and eastern

198   China where anthropogenic emissions are large.

199   We then evaluated the simulated GPP and LAI for the boreal summer period (Fig.

200   2). Observations showed GPP hotspots over boreal forests such as eastern U.S., Eurasia,

201   and East Asia and the tropical forests such as Amazon, central Africa, and Indonesia

202   (Fig. 2b). The seasonal total GPP was estimated to be 41.63Pg[C], which accounted for

203   35% of the annual amount. Simulations well captured the observed GPP pattern on the

204   global scale, with r = 0.63 and NMB = -12.44% over 2581 grids (Fig. 2c), with

205   underestimation in the tundra area and slight overestimation in the tropical rain forest

206   and evergreen forest regions. The model simulated a seasonal total GPP of 36.45 Pg[C],

207   equivalent to 34% of the annual amount. Simulated LAI showed similar patterns as

208   GPP (Fig. 2d) and resembled observed LAI (Fig. 2e) with a high spatial correlation r =

209   0.79 and a low NMB = -5.19% over 4435 grids globally (Fig. 2f).

210   We further validated the simulated meteorology (Fig. S2). For temperature, the

211   model (Fig. S2a) reproduced observed (Fig. S2b) pattern with low NMB of 8.49% and

212   high r of 0.99 against observations (Fig. S2c). For precipitation, both simulations (Fig.

213   S2d) and observations (Fig. S2e) showed high values in the tropical oceans with NMB

214   = 16.91% and r = 0.74 between them (Fig. S2f). Overall, the model showed good

215   performance in the simulations of air pollutants, biospheric parameters, and

216   meteorological fields, and provided a useful tool for studying the O_3-vegetation

217   interactions.

218

3.2 O_3 damage to terrestrial ecosystems

220   We assessed the damaging effects of surface O_3 to ecosystems (Fig. 3). The

221   impacts of O_3 on biospheric variables were mainly located in regions characterized by

222   abundant vegetation cover and elevated O_3 concentrations. On the global scale, O_3

223   induced the GPP reduction of -0.87 PgC yr^{-1} (-3.09%, Fig. 3a). This deleterious effect

224   was more pronounced in specific regions, notably eastern China and eastern U.S., with

225   significant GPP declines of -18.43% and -16.12%, respectively, under high O_3

226   sensitivity conditions (Fig. 3a and Table S2). Meanwhile, stomatal conductance

227   significantly decreased in the middle latitudes of Northern Hemisphere (Fig. 3b). The

228   most substantial relative change of -30.62% was observed in eastern China, followed

9

229   by -25.65% in the eastern U.S. (Fig. 3b and Table S2). These values were stronger than

230   that for GPP (Fig. 3a), likely due to the climatic feedback to O_3-vegetation interactions.

231   The opening of plant stoma plays a crucial role in regulating the energy and water

232   exchange between land surface and the atmosphere. The inhibition of stomatal

233   conductance by surface O_3 leads to the warmer (Fig. 4a) and drier (Fig. 4b) climate in

234   those hotspot regions, resulting in even stronger inhibition effects on stomatal

235   conductance. Following the changes in GPP, global LAI on average decreased by 0.01

236   m^2 m^{-2} (-0.62%) with regional maximums of -4.53% in eastern China and -5.87% in

237   eastern U.S. (Table S2).

238

239   **3.3 Global climatic responses to O_3-vegetation interactions**

240   In response to the O_3-induced inhibition of stomatal conductance, surface air

241   temperature increased by 0.05°C (Fig. 4a) while precipitation decreased by -0.01 mm

242   day^{-1} (Fig. 4b) on the global scale. The most significant change was the warming of

243   0.56°C and precipitation reduction of -0.79 mm day^{-1} (-16.18%) in eastern China (Table

244   S3), following the largest inhibition to stomatal conductance (Fig. 3b). Such warming

245   and rainfall deficit also appeared in eastern U.S. and western Europe, where the O_3-

246   vegetation interactions were notable. The O_3-induced inhibition to stomatal

247   conductance decreased latent heat flux (Fig. 4e) and the consequent precipitation (Fig.

248   4b) in those hotspot regions. Meanwhile, the reduction of latent heat flux promotes

249   surface temperature (Fig. 4a), resulting in the increase of sensible heat flux (Fig. 4f).

250   Such warming was also reported in field experiments, where relatively high O_3

251   exposure resulted in noticeable increases of canopy temperature along with reductions

252   of transpiration (Bernacchi et al., 2011; VanLoocke et al., 2012). Globally, temperature

253   and precipitation showed patchy responses with both positive and negative anomalies,

254   suggesting that the regional hotspots of O_3-induced meteorological changes propagate

255   to surrounding areas through atmospheric perturbations.

256   We further examined the changes in air humidity and cloudiness. Surface relative

257   humidity decreased by 0.18% globally with a similar pattern as that of precipitation

258   (Fig. 4c). The most significant reductions were over eastern China and eastern U.S.,

259   where both the warming (Fig. 4a) and rainfall deficit (Fig. 4b) contributed to the

260   drought. However, in the adjacent regions such as northern China and central U.S., both

261   rainfall and surface relative humidity showed certain enhancement. These changes were

262   associated with the regional increase of cloud cover (Fig. 4d). The sensible heat flux

263   increased by 6.3 W m^{-2} (16.54%) and 7.12 W m^{-2} (25.46%) in eastern U.S. and eastern

264   China, respectively, suggesting a transfer of thermal energy from land to the atmosphere

265   by O_3-vegetation interactions (Fig. 4f and Table S3). The warming effect further

266   triggered anomalous updrafts in the lower troposphere, represented by the changes in

267   vertical velocity (Fig. 5), leading to enhanced convection, reduced atmospheric stability,

268   and consequently an increase in low-level cloudiness (Fig. 4d). However, despite the

269   usual cooling effect associated with increased cloud cover due to reductions in radiation,

270   in regions predominantly influenced by O_3-vegetation interactions, this cooling effect

271   was outweighed by the O_3-induced warming through inhibition of stomatal

272   conductance. Therefore, temperatures exhibited an overall increase of 0.56 °C in

273   eastern China and 0.33 °C in the eastern U.S. (Table S3).

274

3.4 Changes of air pollution by O_3-vegetation interactions

276   Changes in surface water and heat fluxes induced by O_3-vegetation interactions

277   could feed back to affect air pollutants such as O_3 and aerosols. As Fig. 6a and Table

278   S4 show, surface O_3 concentrations enhanced 1.26 ppbv in eastern China and 0.98 ppbv

279   in eastern U.S. due to the decreased dry deposition following O_3 inhibition on stomatal

280   conductance. It indicates that the high contemporary O_3 pollution may worsen air

281   quality through O_3-vegetation interactions. However, negative O_3 changes were

282   predicted in central U.S. and western China, where the increased rainfall dampened O_3

283   through chemical reactions and wet deposition. On a global scale, surface O_3 showed a

284   limited increase of 0.02 ppbv due to the offset between positive and negative feedbacks.

285   The enhancement of O_3 concentrations in polluted regions may exacerbate the warming

286   effect of O_3 and cause additional damages to vegetation.

287   Aerosols also exhibited evident changes by the O_3-vegetation interactions. The

288 AOD showed significant reductions over the hotspot regions such as eastern China and

289 eastern U.S. (Fig. 6b). In the ModelE2-YIBs model, sulfate was especially sensitive to

290 cloud which could enhance the aerosol scavenging through cloud water precipitation

291 (Koch et al., 2006). The large enhancement of cloudiness removed sulfate more

292 efficiently than other aerosol species, leading to an average decline of -1.94 $\mu g\ m^{-3}$ (-

293 8.52%) in $PM_{2.5}$ loading over eastern China (Fig. S3 and Table S4). Meanwhile, the

294 reduction of surface relative humidity (Fig. 4c) in the regions with strong O_3-vegetation

295 interactions limited the hygroscopic growth of aerosols, leading to a more noticeable

296 decrease in AOD (Petters and Kreidenweis, 2007; Revised algorithm for estimating

297 light extinction from IMPROVE particle speciation data, 2023) by -0.06 (-14.67%) in

298 eastern China (Table S4). The similar aerosol changes were found in eastern U.S. but

299 with smaller reductions of $PM_{2.5}$ by -0.27 $\mu g\ m^{-3}$ (-6.01%) and AOD by -0.01 (-8.25%)

300 (Table S4). Beyond the key O_3-vegetation coupling regions, positive but insignificant

301 changes in AOD were predicted, leading to the moderate AOD changes on the global

302 scale (Fig. 6b).

303

304 **4. Conclusions and discussion**

305 We examined the O_3-vegetation feedback to climate and air pollution in the 2010s

306 using the fully coupled climate-carbon-chemistry model ModelE2-YIBs. During boreal

307 summer, surface O_3 resulted in strong damages to GPP and inhibitions to stomatal

308 conductance with regional hotspots over eastern China and eastern U.S. Consequently,

309 surface transpiration was weakened, leading to decreased latent heat fluxes and relative

310 humidity but increased surface air temperature. Meanwhile, the surface warming

311 increased cloud cover by reducing atmospheric stability. The enhancement of

312 cloudiness further decreased surface temperature and promoted precipitation nearby the

313 key regions with intense O_3-vegetation interactions. The O_3-induced inhibition to

314 stomatal conductance resulted in a localized increase in O_3 concentrations. In contrast,

315 the increased cloud cover and decreased relative humidity jointly reduced AOD in

316 hotspot regions. On the global scale, the mean changes of both climate and air pollution

317 were moderate due to the offset between the changes with opposite signs.

Our predicted changes in water/heat fluxes by O_3-vegetation interactions were
consistent with previous studies (Lombardozzi et al., 2015; Arnold et al., 2018; Gong
et al., 2020). For example, the simulations by Lombardozzi et al. (2015) revealed that
surface O_3 reduces global GPP by 8%-12% and transpiration by 2-2.4% with regional
reductions up to 20% for GPP and 15% for transpiration in eastern China and U.S.
These changes were in general consistent with our results though we predicted larger
reductions in transpiration than GPP due to O_3-vegetation interactions. Using the same
scheme as Lombardozzi et al. (2015), Sadiq et al. (2017) showed that O_3-vegetation
coupling induced the surface warming of 0.5-1°C and O_3 enhancement of 4-6 ppbv in
eastern China and eastern U.S. The magnitude of these responses was much stronger
than our predictions. In contrast, the regional simulations by Jin et al. (2023) revealed
that O_3-vegetation coupling led to the increases of temperature up to 0.16°C and surface
O_3 up to 0.6 ppbv in eastern China, both of which were smaller than our predictions.
The damage scheme they use, which depends on cumulative O_3 uptake, omits the
difference in impact on sunlit or shaded leaves and will overestimate the O_3 damage on
GPP compared to the scheme we use, which considers transient O_3 flux (Cao et al.,
2023). The discrepancies of O_3-vegetation feedback using the same O_3 damage schemes
revealed the uncertainties from climate and chemistry models. Our predictions were
within the range of previous estimates for both climatic and O_3 changes.

There were some limitations in our simulated O_3-vegetation interactions. First, the
semi-mechanistic O_3 damage scheme we used in the study linked the damages to
photosynthesis with those to stomatal conductance (Sitch et al., 2007), leading to
stronger inhibition percentage in stomatal conductance than that in photosynthesis
considering the O_3-vegetation feedback. However, some observations showed that the
damage to stomatal conductance occurred more slowly and might not be proportional
to the decline of photosynthetic rates (Gregg et al., 2006; Lombardozzi et al., 2012).
Second, observations have shown large variability of plant sensitivities to O_3 damages.
The Sitch et al. (2007) scheme employed the low to high ranges of sensitivity to indicate
the inter-specific variabilities. In this study, we employed only the high O_3 sensitivity

13

347   to explore the maximum responses. The possible uncertainties due to varied O_3 damage

348   sensitivities deserved further investigations. Third, large-scale observations were not

349   available to validate the simulated regional to global responses of climate and air

350   pollutants. The O_3 vegetation damage scheme was extensively validated against site-

351   level measurements of both photosynthesis (Yue and Unger, 2018) and stomatal

352   conductance (Yue et al., 2016). However, we were conservative about the derived

353   global responses given that previous studies showed large discrepancies using the same

354   O_3 damage scheme but implemented in different climate and/or chemistry models

355   (Lombardozzi et al., 2015; Sadiq et al., 2017; Jin et al., 2023). Furthermore, the 2°×2.5°

356   resolution of current ModelE2-YIBs has limitation due to the high computational

357   demands. Ito et al. (2020) shows that the ModelE2.1 with fixed vegetation traits

358   reproduces carbon fluxes well, and that the model results are involved in the CMIP6

359   Coupled Climate-Carbon Cycle MIP (C4MIP). However, analysis of the climate model

360   shows that high-resolution exhibits improved simulations of extreme events (Chang et

361   al., 2020; Ban et al., 2021), and the application of chemical transport model shows that

362   relatively coarse resolution can raise biases in simulated air pollutants, though it

363   captures the large-scale general pattern almost the same as fine-resolution results and

364   is reasonable as compared to observational data (Wang et al., 2013; Li et al., 2016; Lei

365   et al., 2020). Moreover, we omit the slow climatic feedback caused by air-sea

366   interaction in the simulations. Studies have revealed that these interactions may result

367   in different climatic perturbations from those simulations with fast responses of land

368   surface alone (Yue et al., 2011). A dynamic ocean model is considered to enrich the

369   future research. Meanwhile, this study does not isolate the different impacts of aerosols,

370   even though the radiation module includes both direct and indirect radiative effects. We

371   will investigate this further in the future by identifying the main processes.

372   Despite these uncertainties, our simulations revealed considerable changes of both

373   climate and air pollutants in response to O_3-vegetation interactions. The most intense

374   warming, dryness, and O_3 enhancement were predicted in eastern China and eastern

375   U.S., affecting the regional climate and threatening public health for these top two

376   economic centers. In contrast, we for the first time revealed the reduction of aerosol

377   loading in those hotspot regions, suggesting both positive and negative effects to air

378   pollutants by O_3-vegetation feedback. Such interactions should be considered in the

379   Earth system models so as to better project future changes in climate and air pollutants

380   following the anthropogenic interventions to both O_3 precursor emissions and

381   ecosystem functions.

382

Data Availability

The observational data and model outputs that support the findings in this study are available from corresponding authors upon reasonable request.

Author contributions

XY conceived the project. XZ performed the model simulations, conducted results analysis and wrote the draft manuscript. XY, CT and XL assisted in the interpretation of the results and contributed to the discussion and improvement of the paper.
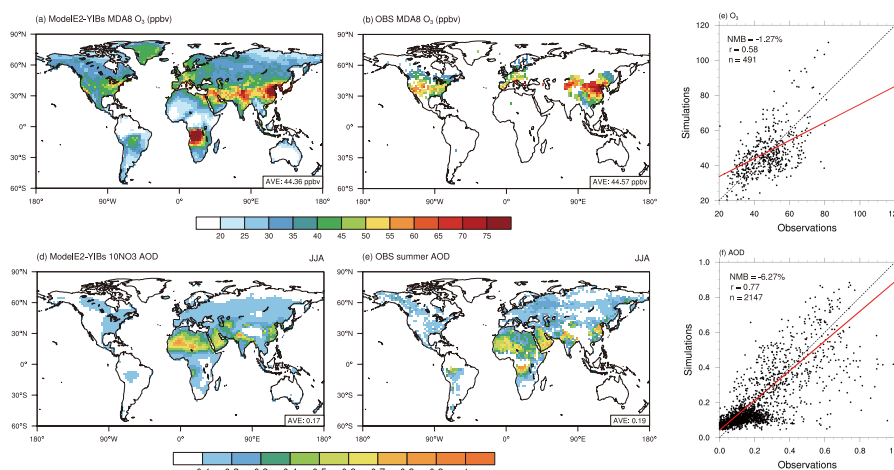
Competing interests

The authors declare that they have no conflict of interest.

Acknowledgments

Figure 1. Evaluation of the boreal summertime (June-August) air pollutants in 2010s simulated by the ModelE2-YIBs model. Surface daily maximum 8-hour ozone (MDA8 O_3, upper) and aerosol optical depth (AOD, bottom) from the simulation 10NO3 (left) and observations (middle) are compared. The correlation coefficients (r), normalized mean bias (NMB), and number of grid cells (n) for the comparisons are listed on the scatter plots (e & f). The dashed line denotes the 1 : 1 ratio. The red line is the linear regression between the simulation and observation.
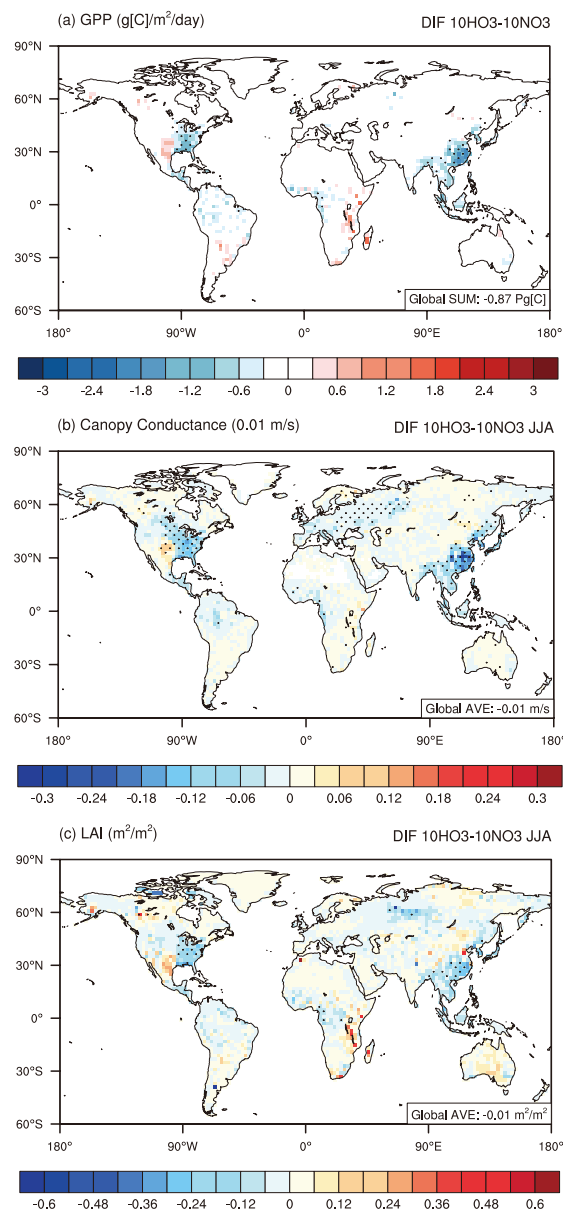
407

408
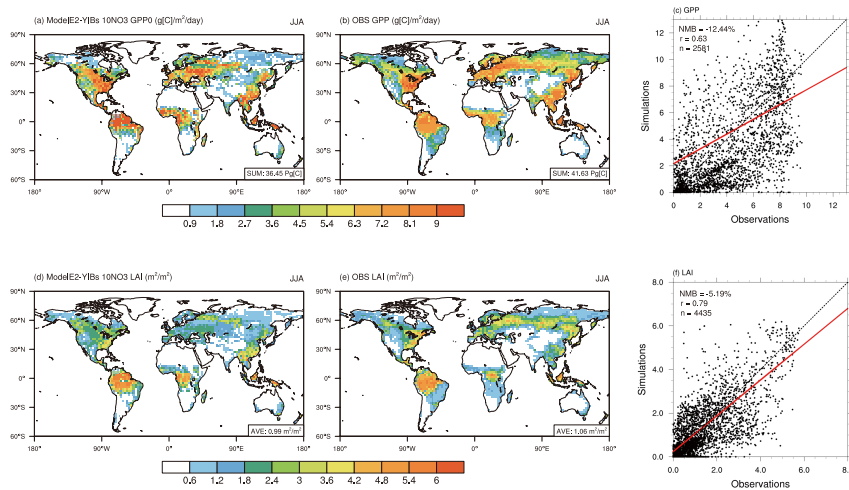
Figure 2. The same as Fig.1 but for gross primary productivity (GPP, upper panels) and
leaf area index (LAI, bottom panels).

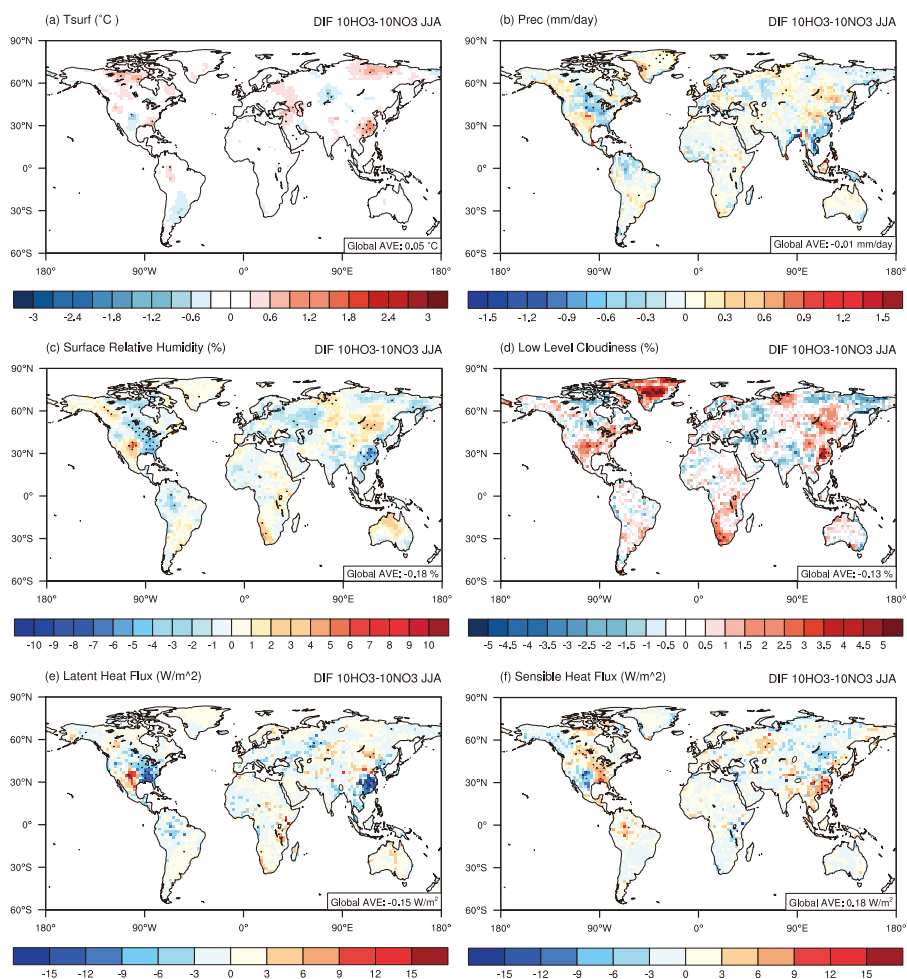**Figure 3.** Changes of boreal summertime biospheric variables induced by O_3 damages in 2010s. Results shown are changes of (a) GPP, (b) canopy conductance, and (c) LAI between simulatio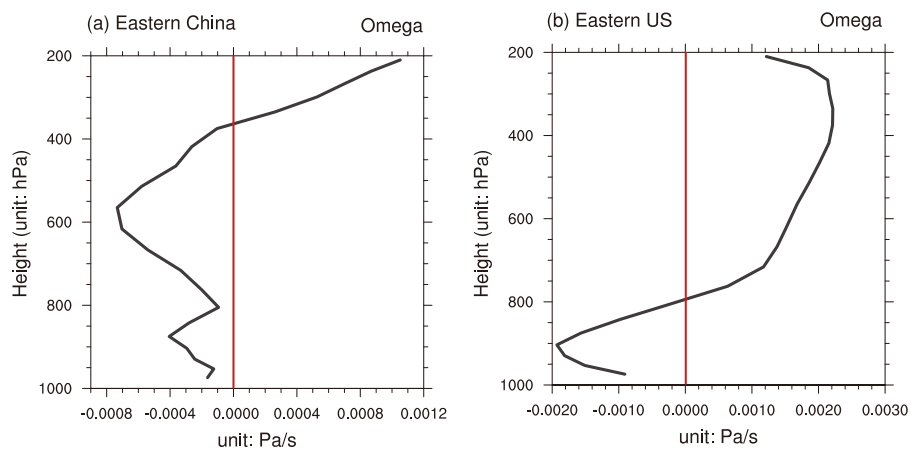ns 10HO3 and 10NO3. Black dots denote areas with significant changes ($p < 0.1$). Please notice the differences in the color scales.

Figure 4. Changes of boreal summertime meteorological fields by ozone-vegetation interactions in 2010s. Results shown are changes of (a) surface temperature, (b) precipitation, (c) surface relative humidity, (d) low level cloudiness, (e) latent heat flux, and (f) sensible heat flux between simulations 10HO3 and 10NO3. For heat fluxes, positive values (shaded in red color) indicate the upward fluxes change. Black dots denote areas with significant changes ($p < 0.1$). Please notice the differences in the color scales.
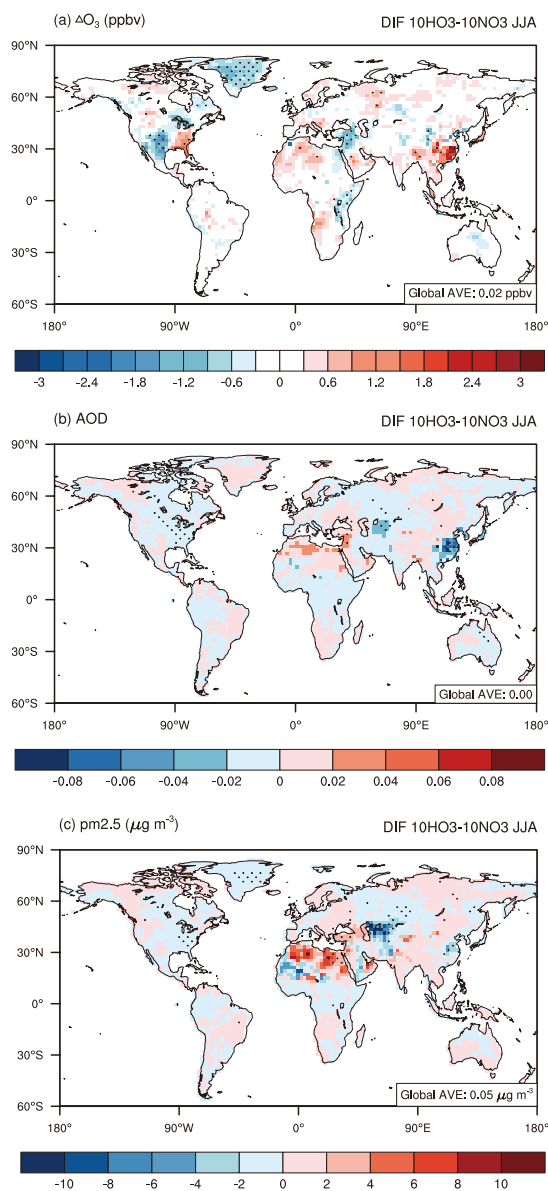
424

Figure 5. Vertical profile of vertical velocity. Results shown are changes of the vertical velocity in (a) Eastern China and (b) Eastern US between simulations 10HO3 and 10NO3. Solid red line denotes the value 0. Please notice the differences in the scales.

430
Fig. 6. Changes of summertime atmospheric pollution caused by ozone-vegetation
interactions in 2010s. Results shown are changes of (a) ozone, (b) AOD, and (c) **PM$_{2.5}$**
between 10HO3 and 10NO3. Black dots denote areas with significant changes ($p < 0.1$).
Please notice the differences in the color scales.

435

References

Adler, R. F., Sapiano, M. R. P., Huffman, G. J., Wang, J.-J., Gu, G., Bolvin, D., Chiu, L., Schneider, U., Becker, A., Nelkin, E., Xie, P., Ferraro, R., and Shin, D.-B.: The Global Precipitation Climatology Project (GPCP) Monthly Analysis (New Version 2.3) and a Review of 2017 Global Precipitation, Atmosphere, 9, 138, https://doi.org/10.3390/atmos9040138, 2018.

Ainsworth, E. A., Yendrek, C. R., Sitch, S., Collins, W. J., and Emberson, L. D.: The effects of tropospheric ozone on net primary productivity and implications for climate change, Annu. Rev. Plant. Biol., 63, 637–661, https://doi.org/10.1146/annurev-arplant-042110-103829, 2012.

Anav, A., Menut, L., Khvorostyanov, D., and Viovy, N.: Impact of tropospheric ozone on the Euro-Mediterranean vegetation, Glob. Change. Biol., 17, 2342–2359, https://doi.org/10.1111/j.1365-2486.2010.02387.x, 2011.

Arnold, S. R., Lombardozzi, D., Lamarque, J. -F., Richardson, T., Emmons, L. K., Tilmes, S., Sitch, S. A., Folberth, G., Hollaway, M. J., and Val Martin, M.: Simulated Global Climate Response to Tropospheric Ozone-Induced Changes in Plant Transpiration, Geophys. Res. Lett., 45, 13070–13079, https://doi.org/10.1029/2018GL079938, 2018.

Ball, J. T., Woodrow, I. E., and Berry, J. A.: A Model Predicting Stomatal Conductance and its Contribution to the Control of Photosynthesis under Different Environmental Conditions, in: Progress in Photosynthesis Research, edited by: Biggins, J., Springer Netherlands, Dordrecht, 221–224, https://doi.org/10.1007/978-94-017-0519-6_48, 1987.

Ban, N., Caillaud, C., Coppola, E., Pichelli, E., Sobolowski, S., Adinolfi, M., Ahrens, B., Alias, A., Anders, I., Bastin, S. and Belušić, D.: The first multi-model ensemble of regional climate simulations at kilometer-scale resolution, part I: evaluation of precipitation, Clim. Dynam., 57, 275-302, https://doi.org/10.1007/s00382-021-05708-w, 2021.

Bernacchi, C. J., Leakey, A. D. B., Kimball, B. A., and Ort, D. R.: Growth of soybean at future tropospheric ozone concentrations decreases canopy evapotranspiration and soil water depletion, Environ. Pollut., 159, 1464–1472, https://doi.org/10.1016/j.envpol.2011.03.011, 2011.

Cao, J., Yue, X. and Ma, M.: Simulation of ozone-vegetation coupling and feedback in China using multiple ozone damage schemes, Atmos. Chem. Phys., 24(7), 3973-3987, https://doi.org/10.5194/acp-24-3973-2024, 2024.

Chang, P., Zhang, S., Danabasoglu, G., Yeager, S.G., Fu, H., Wang, H., Castruccio, F.S., Chen, Y., Edwards, J., Fu, D. and Jia, Y.: An unprecedented set of high-resolution earth system simulations for understanding multiscale interactions in climate

474   variability   and   change,   J.   Adv.   Model.   Earth.   Sy.,   12,
475   https://doi.org/10.1029/2020MS002298, 2020.

476   Clifton, O. E., Paulot, F., Fiore, A. M., Horowitz, L. W., Correa, G., Baublitz, C. B.,
477   Fares, S., Goded, I., Goldstein, A. H., Gruening, C., Hogg, A. J., Loubet, B.,
478   Mammarella, I., Munger, J. W., Neil, L., Stella, P., Uddling, J., Vesala, T., and
479   Weng, E.: Influence of Dynamic Ozone Dry Deposition on Ozone Pollution, J.
480   Geophys.   Res-Atmos,   125,   e2020JD032398,
481   https://doi.org/10.1029/2020JD032398, 2020.

482   Dizengremel, P.: Effects of ozone on the carbon metabolism of forest trees, Plant.
483   Physiol. Bioch., 39, 729–742, https://doi.org/10.1016/S0981-9428(01)01291-8,
484   2001.

485   Farquhar, G. D., von Caemmerer, S., and Berry, J. A.: A biochemical model of
486   photosynthetic CO_2 assimilation in leaves of C_3 species, Planta, 149, 78–90,
487   https://doi.org/10.1007/BF00386231, 1980.

488   Fiscus, E. L., Booker, F. L., and Burkey, K. O.: Crop responses to ozone: uptake, modes
489   of action, carbon assimilation and partitioning, Plant. Cell. Environ., 28, 997–1011,
490   https://doi.org/10.1111/j.1365-3040.2005.01349.x, 2005.

491   Fuhrer, J., Skärby, L. and Ashmore, M.R.: Critical levels for ozone effects on vegetation
492   in Europe, Environ. Pollut., 97, 91-106, https://doi.org/10.1016/S0269-
493   7491(97)00067-5, 1997.

494   Gong, C., Lei, Y., Ma, Y., Yue, X., and Liao, H.: Ozone–vegetation feedback through
495   dry deposition and isoprene emissions in a global chemistry–carbon–climate
496   model, Atmos. Chem. Phys., 20, 3841–3857, https://doi.org/10.5194/acp-20-
497   3841-2020, 2020.

498   Gregg, J. W., Jones, C. G., and Dawson, T. E.: Physiological and Developmental Effects
499   of O_3 on Cottonwood Growth in Urban and Rural Sites, Ecol. Appl., 16, 2368–
500   2381,   https://doi.org/10.1890/1051-0761(2006)016[2368:PADEOO]2.0.CO;2,
501   2006.

502   Hoesly, R. M., Smith, S. J., Feng, L., Klimont, Z., Janssens-Maenhout, G., Pitkanen, T.,
503   Seibert, J. J., Vu, L., Andres, R. J., Bolt, R. M., Bond, T. C., Dawidowski, L.,
504   Kholod, N., Kurokawa, J., Li, M., Liu, L., Lu, Z., Moura, M. C. P., O'Rourke, P.
505   R., and Zhang, Q.: Historical (1750–2014) anthropogenic emissions of reactive
506   gases and aerosols from the Community Emissions Data System (CEDS), Geosci.
507   Model. Dev., 11, 369–408, https://doi.org/10.5194/gmd-11-369-2018, 2018.

508   Huffman, G. J., Adler, R. F., Arkin, P., Chang, A., Ferraro, R., Gruber, A., Janowiak, J.,
509   McNab, A., Rudolf, B., and Schneider, U.: The Global Precipitation Climatology
510   Project (GPCP) Combined Precipitation Dataset, B. Am. Meteorol. Soc., 78, 5–20,

511   https://doi.org/10.1175/1520-0477(1997)078<0005:TGPCPG>2.0.CO;2, 1997.

512   Hurtt, G. C., Chini, L., Sahajpal, R., Frolking, S., Bodirsky, B. L., Calvin, K., Doelman,
513   J. C., Fisk, J., Fujimori, S., Klein Goldewijk, K., Hasegawa, T., Havlik, P.,
514   Heinimann, A., Humpenöder, F., Jungclaus, J., Kaplan, J. O., Kennedy, J., Krisztin,
515   T., Lawrence, D., Lawrence, P., Ma, L., Mertz, O., Pongratz, J., Popp, A., Poulter,
516   B., Riahi, K., Shevliakova, E., Stehfest, E., Thornton, P., Tubiello, F. N., van
517   Vuuren, D. P., and Zhang, X.: Harmonization of global land use change and
518   management for the period 850–2100 (LUH2) for CMIP6, Geosci. Model. Dev.,
519   13, 5425–5464, https://doi.org/10.5194/gmd-13-5425-2020, 2020.

520   Ito, G., Romanou, A., Kiang, N.Y., Faluvegi, G., Aleinov, I., Ruedy, R., Russell, G.,
521   Lerner, P., Kelley, M. and Lo, K.: Global carbon cycle and climate feedbacks in
522   the NASA GISS ModelE2, J. Adv. Model. Earth. Sy., 12, https://doi.org/
523   10.1029/2019MS002030, 2020.

524   Jin, Z., Yan, D., Zhang, Z., Li, M., Wang, T., Huang, X., Xie, M., Li, S., and Zhuang,
525   B.: Effects of Elevated Ozone Exposure on Regional Meteorology and Air Quality
526   in China Through Ozone-Vegetation Coupling, J. Geophys. Res-Atmos., 128,
527   e2022JD038119, https://doi.org/10.1029/2022JD038119, 2023.

528   Jolivet, Y., Bagard, M., Cabané, M., Vaultier, M.-N., Gandin, A., Afif, D., Dizengremel,
529   P., and Le Thiec, D.: Deciphering the ozone-induced changes in cellular processes:
530   a prerequisite for ozone risk assessment at the tree and forest levels, Ann. For. Sci.,
531   73, 923–943, https://doi.org/10.1007/s13595-016-0580-3, 2016.

532   Jung, M., Reichstein, M., and Bondeau, A.: Towards global empirical upscaling of
533   FLUXNET eddy covariance observations: validation of a model tree ensemble
534   approach using a biosphere model, Biogeosciences, 6, 2001–2013, 2009.

535   Kalnay, E., Kanamitsu, M., Kistler, R., Collins, W., Deaven, D., Gandin, L., Iredell, M.,
536   Saha, S., White, G., Woollen, J., Zhu, Y., Chelliah, M., Ebisuzaki, W., Higgins, W.,
537   Janowiak, J., Mo, K. C., Ropelewski, C., Wang, J., Leetmaa, A., Reynolds, R.,
538   Jenne, R., and Joseph, D.: The NCEP/NCAR 40-Year Reanalysis Project, B. Am.
539   Meteorol.   Soc.,   77,   437–472,   https://doi.org/10.1175/1520-
540   0477(1996)077<0437:TNYRP>2.0.CO;2, 1996.

541   Karlsson, P., Uddling, J., Braun, S., Broadmeadow, M., Elvira, S., Gimeno, B., Le Thiec,
542   D., Oksanen, E., Vandermeiren, K., Wilkinson, M., and Emberson, L.: New critical
543   levels for ozone effects on young trees based on AOT40 and simulated cumulative
544   leaf   uptake   of   ozone,   Atmos.   Environ.,   38,   2283–2294,
545   https://doi.org/10.1016/j.atmosenv.2004.01.027, 2004.

546   Koch, D., Schmidt, G. A., and Field, C. V.: Sulfur, sea salt, and radionuclide aerosols
547   in   GISS   ModelE,   J.   Geophys.   Res-Atmos,   111,
548   https://doi.org/10.1029/2004JD005550, 2006.

Lam, J. C. Y., Tai, A. P. K., Ducker, J. A., and Holmes, C. D.: Development of an ecophysiology module in the GEOS-Chem chemical transport model version 12.2.0 to represent biosphere–atmosphere fluxes relevant for ozone air quality, Geosci. Model. Dev., 16, 2323–2342, https://doi.org/10.5194/gmd-16-2323-2023, 2023.

Lei, Y., Yue, X., Liao, H., Gong, C., and Zhang, L.: Implementation of Yale Interactive terrestrial Biosphere model v1.0 into GEOS-Chem v12.0.0: a tool for biosphere–chemistry interactions, Geosci. Model. Dev., 13, 1137–1153, https://doi.org/10.5194/gmd-13-1137-2020, 2020.

Lei, Y., Yue, X., Liao, H., Zhang, L., Yang, Y., Zhou, H., Tian, C., Gong, C., Ma, Y., and Gao, L.: Indirect contributions of global fires to surface ozone through ozone–vegetation feedback, Atmos. Chem. Phys., 21, 11531–11543, https://doi.org/10.5194/acp-21-11531-2021. 2021.

Li, Y., Henze, D.K., Jack, D.: The influence of air quality model resolution on health impact assessment for fine particulate matter and its components, Air. Qual. Atmos. Hlth., 9, 51-68, https://doi.org/10.1007/s11869-015-0321-z, 2016.

Lombardozzi, D., Levis, S., Bonan, G., and Sparks, J. P.: Predicting photosynthesis and transpiration responses to ozone: decoupling modeled photosynthesis and stomatal conductance, Biogeosciences, 9, 3113–3130, https://doi.org/10.5194/bg-9-3113-2012, 2012.

Lombardozzi, D., Sparks, J. P., and Bonan, G.: Integrating O_3 influences on terrestrial processes: photosynthetic and stomatal response data available for regional and global modeling, Biogeosciences, 10, 6815–6831, https://doi.org/10.5194/bg-10-6815-2013, 2013.

Lombardozzi, D., Levis, S., Bonan, G., Hess, P. G., and Sparks, J. P.: The Influence of Chronic Ozone Exposure on Global Carbon and Water Cycles, J. Climate., 28, 292–305, https://doi.org/10.1175/JCLI-D-14-00223.1, 2015.

van Marle, M. J. E., Kloster, S., Magi, B. I., Marlon, J. R., Daniau, A.-L., Field, R. D., Arneth, A., Forrest, M., Hantson, S., Kehrwald, N. M., Knorr, W., Lasslop, G., Li, F., Mangeon, S., Yue, C., Kaiser, J. W., and van der Werf, G. R.: Historic global biomass burning emissions for CMIP6 (BB4CMIP) based on merging satellite observations with proxies and fire models (1750–2015), Geosci. Model. Dev., 10, 3329–3357, https://doi.org/10.5194/gmd-10-3329-2017, 2017.

Menon, S. and Rotstayn, L.: The radiative influence of aerosol effects on liquid-phase cumulus and stratiform clouds based on sensitivity studies with two climate models, Clim. Dyn., 27, 345–356, https://doi.org/10.1007/s00382-006-0139-3, 2006.

586 Mills, G., Buse, A., Gimeno, B., Bermejo, V., Holland, M., Emberson, L., and Pleijel,
587   H.: A synthesis of AOT40-based response functions and critical levels of ozone
588   for agricultural and horticultural crops, Atmos. Environ., 41, 2630–2643,
589   https://doi.org/10.1016/j.atmosenv.2006.11.016 , 2007.

590 Myhre, G., Shindell, D., Breìon, F.-M., Collins, W., Fuglestvedt, J., Huang, J., Koch,
591   D., Lamarque, J.-F., Lee, D., Mendoza, B., Nakajima, T., Robock, A., Stephens,
592   G., Takemura, T., and Zhang, H., Anthropogenic and Natural Radiative Forcing,
593   in: Climate Change 2013: The Physical Science Basis. Contribution of Working
594   Group I to the Fifth Assessment Report of the Intergovernmental Panel on Climate
595   Change, edited by: Stocker, T. F., Qin, D., Plattner, G.-K., Tignor, M., Allen, S. K.,
596   Boschung, J., Nauels, A., Xia, Y., Bex, V., and Midgley, P. M., Cambridge
597   University Press, Cambridge, UK and New York, NY, USA, 2013.

598 Norval, M., Lucas, R. M., Cullen, A. P., De Gruijl, F. R., Longstreth, J., Takizawa, Y.,
599   and Van Der Leun, J. C.: The human health effects of ozone depletion and
600   interactions with climate change, Photoch. Photobio. Sci., 10, 199–225,
601   https://doi.org/10.1039/C0PP90044C, 2011.

602 Nussbaum, S. and Fuhrer, J.: Difference in ozone uptake in grassland species between
603   open-top chambers and ambient air, Environ. Pollut., 109, 463–471,
604   https://doi.org/10.1016/S0269-7491(00)00049-X, 2000.

605 Nuvolone, D., Petri, D., and Voller, F.: The effects of ozone on human health, Environ.
606   Sci. Pollut. R., 25, 8074–8088, https://doi.org/10.1007/s11356-017-9239-3, 2018.

607 Ohara, T., Akimoto, H., Kurokawa, J., Horii, N., Yamaji, K., Yan, X., and Hayasaka, T.:
608   An Asian emission inventory of anthropogenic emission sources for the period
609   1980-2020, Atmos. Chem. Phys., 7, 4419–4444, https://doi.org/10.5194/acp-7-
610   4419-2007, 2007.

611 Oliver, R. J., Mercado, L. M., Sitch, S., Simpson, D., Medlyn, B. E., Lin, Y.-S., and
612   Folberth, G. A.: Large but decreasing effect of ozone on the European carbon sink,
613   Biogeosciences, 15, 4245–4269, 2018.

614 Petters, M. D. and Kreidenweis, S. M.: A single parameter representation of
615   hygroscopic growth and cloud condensation nucleus activity, Atmos. Chem. Phys.,
616   7, 1961–1971, https://doi.org/10.5194/acp-7-1961-2007, 2007.

617 Pitchford, M., Malm, W., Schichtel, B., Kumar, N., Lowenthal, D., and Hand, J.:
618   Revised Algorithm for Estimating Light Extinction from IMPROVE Particle
619   Speciation Data, Japca. J. Air. Waste. Ma., 57 (11), 1326–1336,
620   https://doi.org/10.3155/1047-3289.57.11.1326, 2007.

621 Pleijel, H., Danielsson, H., Ojanperä, K., Temmerman, L. D., Högy, P., Badiani, M.,
622   and Karlsson, P. E.: Relationships between ozone exposure and yield loss in

623   European wheat and potato—a comparison of concentration- and flux-based
624   exposure indices, Atmos. Environ., 38, 2259–2269,
625   https://doi.org/10.1016/j.atmosenv.2003.09.076, 2004.

626 Pleijel, H., Danielsson, H., Emberson, L., Ashmore, M. R., and Mills, G.: Ozone risk
627   assessment for agricultural crops in Europe: further development of stomatal flux
628   and flux–response relationships for European wheat and potato, Atmos. Environ.,
629   41, 3022–3040, https://doi.org/10.1016/j.atmosenv.2006.12.002, 2007.

630 Remer, L. A., Kaufman, Y. J., Tanré, D., Mattoo, S., Chu, D. A., Martins, J. V., Li, R.-
631   R., Ichoku, C., Levy, R. C., and Kleidman, R. G.: The MODIS aerosol algorithm,
632   products, and validation, J. Atmos. Sci., 62, 947–973,
633   https://doi.org/10.1175/JAS3385.1, 2005.

634 Sadiq, M., Tai, A. P., Lombardozzi, D., and Val Martin, M.: Effects of ozone–vegetation
635   coupling on surface ozone air quality via biogeochemical and meteorological
636   feedbacks, Atmos. Chem. Phys., 17, 3055–3066, https://doi.org/10.5194/acp-17-
637   3055-2017, 2017.

638 Schmidt, G. A., Ruedy, R., Hansen, J. E., Aleinov, I., Bell, N., Bauer, M., Bauer, S.,
639   Cairns, B., Canuto, V., Cheng, Y., Genio, A. D., Faluvegi, G., Friend, A. D., Hall,
640   T. M., Hu, Y., Kelley, M., Kiang, N. Y., Koch, D., Lacis, A. A., Lerner, J., Lo, K.
641   K., Miller, R. L., Nazarenko, L., Oinas, V., Perlwitz, J., Perlwitz, J., Rind, D.,
642   Romanou, A., Russell, G. L., Sato, M., Shindell, D. T., Stone, P. H., Sun, S.,
643   Tausnev, N., Thresher, D., and Yao, M.-S.: Present-Day Atmospheric Simulations
644   Using GISS ModelE: Comparison to In Situ, Satellite, and Reanalysis Data, J.
645   Climate., 19, 153–192, https://doi.org/10.1175/JCLI3612.1, 2006.

646 Schmidt, G. A., Kelley, M., Nazarenko, L., Ruedy, R., Russell, G. L., Aleinov, I., Bauer,
647   M., Bauer, S. E., Bhat, M. K., Bleck, R., Canuto, V., Chen, Y.-H., Cheng, Y., Clune,
648   T. L., Del Genio, A., de Fainchtein, R., Faluvegi, G., Hansen, J. E., Healy, R. J.,
649   Kiang, N. Y., Koch, D., Lacis, A. A., LeGrande, A. N., Lerner, J., Lo, K. K.,
650   Matthews, E. E., Menon, S., Miller, R. L., Oinas, V., Oloso, A. O., Perlwitz, J. P.,
651   Puma, M. J., Putman, W. M., Rind, D., Romanou, A., Sato, M., Shindell, D. T.,
652   Sun, S., Syed, R. A., Tausnev, N., Tsigaridis, K., Unger, N., Voulgarakis, A., Yao,
653   M.-S., and Zhang, J.: Configuration and assessment of the GISS ModelE2
654   contributions to the CMIP5 archive: GISS MODEL-E2 CMIP5 SIMULATIONS,
655   J. Adv. Model. Earth Syst., 6, 141–184, https://doi.org/10.1002/2013MS000265,
656   2014.

657 Sitch, S., Cox, P. M., Collins, W. J., and Huntingford, C.: Indirect radiative forcing of
658   climate change through ozone effects on the land-carbon sink, Nature, 448, 791–
659   794, https://doi.org/10.1038/nature06059, 2007.

660 Unger, N., Zheng, Y., Yue, X., and Harper, K. L.: Mitigation of ozone damage to the
661   world's land ecosystems by source sector, Nat. Clim. Chang., 10, 134–137,

662   https://doi.org/10.1038/s41558-019-0678-3, 2020.

663   VanLoocke, A., Betzelberger, A. M., Ainsworth, E. A., and Bernacchi, C. J.: Rising
664   ozone concentrations decrease soybean evapotranspiration and water use
665   efficiency whilst increasing canopy temperature, New. Phytol., 195, 164–171,
666   https://doi.org/10.1111/j.1469-8137.2012.04152.x, 2012.

667   van der Werf, G. R., Randerson, J. T., Giglio, L., van Leeuwen, T. T., Chen, Y., Rogers,
668   B. M., Mu, M., van Marle, M. J. E., Morton, D. C., Collatz, G. J., Yokelson, R. J.,
669   and Kasibhatla, P. S.: Global fire emissions estimates during 1997–2016, Earth.
670   Syst. Sci. Data, 9, 697–720, https://doi.org/10.5194/essd-9-697-2017, 2017.

671   Wang, Y., Shen, L., Wu, S., Mickley, L., He, J. and Hao, J.: Sensitivity of surface ozone
672   over China to 2000–2050 global changes of climate and emissions, Atmos.
673   Environ, 75, 374-382, https://doi.org/10.1016/j.atmosenv.2013.04.045, 2013.

674   Wesely, M. L. and Hicks, B. B.: A review of the current status of knowledge on dry
675   deposition, Atmos. Environ., 34, 2261–2282, https://doi.org/10.1016/S1352-
676   2310(99)00467-7, 2000.

677   Wild, M., Folini, D., Schär, C., Loeb, N., Dutton, E. G., and König-Langlo, G.: The
678   global energy balance from a surface perspective, Clim. Dyn., 40, 3107–3134,
679   https://doi.org/10.1007/s00382-012-1569-8, 2013.

680   Yue, X., Liao, H., Wang, H. J., Li, S. L., and Tang, J. P.: Role of sea surface temperature
681   responses in simulation of the climatic effect of mineral dust aerosol, Atmos.
682   Chem. Phys., 11, 6049-6062, https://doi.org/10.5194/acp-11-6049-2011, 2011.

683   Yue, X. and Unger, N.: Ozone vegetation damage effects on gross primary productivity
684   in the United States, Atmos. Chem. Phys., 14, 9137–9153,
685   https://doi.org/10.5194/acp-14-9137-2014, 2014.

686   Yue, X. and Unger, N.: The Yale Interactive terrestrial Biosphere model version 1.0:
687   description, evaluation and implementation into NASA GISS ModelE2, Geosci.
688   Model Dev., 8, 2399–2417, https://doi.org/10.5194/gmd-8-2399-2015, 2015.

689   Yue, X. and Unger, N.: Fire air pollution reduces global terrestrial productivity, Nat.
690   Commun., 9, 5413, https://doi.org/10.1038/s41467-018-07921-4, 2018.

691   Yue, X., Keenan, T. F., Munger, W., and Unger, N.: Limited effect of ozone reductions
692   on the 20-year photosynthesis trend at Harvard forest, Glob. Change Biol., 22,
693   3750–3759, https://doi.org/10.1111/gcb.13300, 2016.

694   Yue, X., Liao, H., Wang, H., Zhang, T., Unger, N., Sitch, S., Feng, Z., and Yang, J.:
695   Pathway dependence of ecosystem responses in China to 1.5°C global warming,
696   Atmos. Chem. Phys., 20, 2353–2366, https://doi.org/10.5194/acp-20-2353-2020,
697   2020.

698   Zhang, L., Vet, R., Brook, J. R., and Legge, A. H.: Factors affecting stomatal uptake of
699   ozone by different canopies and a comparison between dose and exposure, Sci.
700   Total Environ., 370, 117–132, https://doi.org/10.1016/j.scitotenv.2006.06.004,
701   2006.

702   Zhou, X., Yue, X., and Tian, C.: Responses of Ecosystem Productivity to Anthropogenic
703   Ozone and Aerosols at the 2060, Earths Future, 12, e2023EF003781,
704   https://doi.org/10.1029/2023EF003781, 2024.

705   Zhu, J., Tai, A. P. K., and Hung Lam Yim, S.: Effects of ozone–vegetation interactions
706   on meteorology and air quality in China using a two-way coupled land–
707   atmosphere model, Atmos. Chem. Phys., 22, 765–782,
708   https://doi.org/10.5194/acp-22-765-2022, 2022.

709